

Illustrations

Chapter 0

- Figure 0-1:** *General approach taken by the Belgian methodological research and development programme into deep disposal..... 23*
- Figure 0-2:** *Implicit technical choices made within the methodological R&D programme and within SAFIR 2 (in blue); alternative options are indicated in red. 24*

Chapter 1

- Figure 1-1:** *Schematic concept of the potential options for the long-term management of radioactive waste. 25*
- Figure 1-2:** *Illustration of the successive phases in the development and implementation of a disposal solution for conditioned high-level and long-lived waste with indicated time scales for a disposal in the Boom Clay Formation..... 26*
- Figure 1-3:** *Comparison of release to the biosphere resulting from the two management options ‘dilute and disperse’ and ‘concentrate and contain’ (by disposal). 27*
- Figure 1-4:** *Mean annual natural exposure in a number of countries and comparison with the dose limit and dose constraint..... 28*
- Figure 1-5:** *The various components and main barriers of the disposal facility and the disposal system..... 28*
- Figure 1-6:** *Relative activity of a spent nuclear fuel (burn-up of 45 MWd/kg U) and comparison with the activity of an equivalent amount of uranium ore [25]. The short-lived radionuclides are not considered in this figure 29*
- Figure 1-7:** *Schematic representation of the two approaches to site selection discussed in the text. The phase in **Figure 1-2** corresponding to each step in the selection process is also given. 30*

Chapter 2

--

Chapter 3

<u>Figure 3-1:</u>	<i>Extent of favourable geological formations as defined in the EC Catalogue [5].....</i>	<i>31</i>
<u>Figure 3-2:</u>	<i>Extent of the delineated investigation area for the Boom Clay. This area as defined here and further on includes the area defined by [22] and the extension to the north.</i>	<i>32</i>
<u>Figure 3-3:</u>	<i>Extent of the delineated investigation area for the Ypresian Clays.</i>	<i>33</i>
<u>Figure 3-4:</u>	<i>The Belgian position on the selection of host formations and sites (the options studied by ONDRAF/NIRAS and covered by SAFIR 2 are shown in continuous lines; the dotted line boxes show the options and choices which require public dialogue).....</i>	<i>34</i>
<u>Figure 3-5:</u>	<i>Chrono- and lithostratigraphic position of the Boom Clay.</i>	<i>35</i>
<u>Figure 3-6:</u>	<i>Transgressions and regressions in the Oligocene, indicating the various lithostratigraphic units.....</i>	<i>35</i>
<u>Figure 3-7:</u>	<i>The Boom Clay at Kruibekke: the silt layers are light in colour, the clay layers are dark.</i>	<i>35</i>
<u>Figure 3-8:</u>	<i>Lithostratigraphic profile of the Boom Clay and lithological variables based on field observations. Mfs: maximum flooding surface (grain size minimum); db: dubbel layer, showing a grain size maximum (beds 39 and 41).</i>	<i>36</i>
<u>Figure 3-9:</u>	<i>Outcrop and subcrop of the Boom Clay also showing depth to base relative to sea level and thickness.</i>	<i>37</i>
<u>Figure 3-10:</u>	<i>East-west profile Lommel – Olmen modified according to [25]. Location of the profile is shown in Figure 3-9.</i>	<i>38</i>
<u>Figure 3-11:</u>	<i>The boundaries of the investigation area superimposed onto the administrative map of Belgium.</i>	<i>39</i>
<u>Figure 3-12:</u>	<i>Morphological division of the Campine (modified according to [35], and [36]). I: Northern Campine (cuesta of the Campine clays); II: Central Campine (IIa: the Brasschaat glacis; IIb: the Schijns-Nete depression; IIbl: the Lichtaard ridge; IIbg: the Geel ridge); III: Southern Campine (IIIa: the sub-cuesta of Heist-op-den-Berg; IIIb: eastern spur of the Flemish Valley); IV(a): the Campine Plateau (IVb: the Beringen-Diepenbeek glacis).....</i>	<i>40</i>

<u>Figure 3-13:</u>	<i>Distribution of Pasquill stability classes (%) for 1989 at Mol. F is the most stable situation, D represents a neutral situation and A is the least stable situation.....</i>	41
<u>Figure 3-14:</u>	<i>Overview of the hydrology of the Campine, showing gradients and basin sizes.</i>	41
<u>Figure 3-15:</u>	<i>Stratigraphic and lithological successions in the Campine Basin [25].</i>	42
<u>Figure 3-16:</u>	<i>Generalised block diagram of the Tertiary and Cretaceous Formations in the Campine Basin (modified from [25]).</i>	43
<u>Figure 3-17:</u>	<i>Elevation variations in mm between 1948 and 1980 relative to the reference geodetic point at Uccle [38].</i>	44
<u>Figure 3-18:</u>	<i>Fault and depth map of the base of the Miocene with additional data from the Mol sheet of the geological map [34].</i>	45
<u>Figure 3-19:</u>	<i>General map of the instrumental seismicity in Belgium (Richter scale magnitudes [45]).</i>	46
<u>Figure 3-20:</u>	<i>Countours of earthquake intensity (MSK scale) in Belgium and neighbouring areas during the 19th and 20th centuries, modified from [36].</i>	47
<u>Figure 3-21:</u>	<i>Extent of the different aquifers in north-eastern Belgium (maps developed from [47, 48]).</i>	48
<u>Figure 3-22:</u>	<i>Schematic overview of the Tertiary and Quaternary aquifers and aquitards in the Campine Basin.</i>	49
<u>Figure 3-23:</u>	<i>Temperature distribution in Belgium at a depth of 500 m, and indication of the different formations suitable for geothermal energy production (modified according to [57]).</i>	50
<u>Figure 3-24:</u>	<i>Mineral resources of the Campine Basin.</i>	51
<u>Figure 3-25:</u>	<i>Total spectrometer image (U, Th, K) of Belgium (units in count per second) [61].</i>	52
<u>Figure 3-26:</u>	<i>Location map of seismic survey 3D-78 and the associated test 2, the 96-ON seismic survey and the SCK-15, Dessel-1 and Mol-1 boreholes. Line 96-14 was shot at the same place as test line 91-ON-01.</i>	53
<u>Figure 3-27:</u>	<i>Stratigraphy of the Dessel-1 borehole</i>	54
<u>Figure 3-28:</u>	<i>Stratigraphy of the Mol-1 borehole.</i>	55

<u>Figure 3-29:</u>	<i>Position of the samples taken from the Mol-1 borehole (M 1-12: regular intervals of 10 m; M 13-20: special samples; MTP 1-20: regular intervals of 50 cm at the base of the Putte Member).....</i>	<i>56</i>
<u>Figure 3-30:</u>	<i>Natural radioactivity of ⁴⁰K and ⁸⁷Rb in the Boom Clay.</i>	<i>56</i>
<u>Figure 3-31:</u>	<i>Natural radioactivity of ²²⁶Ra, ²²⁸Ra, ²³⁴U, ²³⁸U, ²³²Th, ²³⁰Th and ²²⁸Th in the Boom Clay.</i>	<i>57</i>
<u>Figure 3-32:</u>	<i>Correlation of Dessel-1 borehole with SCK-15 borehole.....</i>	<i>58</i>
<u>Figure 3-33:</u>	<i>Stratigraphic correlation based on the presence of septaria levels between the Mol-1 borehole and the observations made during the construction of the new shaft (shaft 2, PRACLAY project).</i>	<i>59</i>
<u>Figure 3-34:</u>	<i>Interpreted seismic line 96-01 through the Boom Clay: red: base of the 'transition layer', yellow: 'double layer'; blue: base of the Terhagen Member. The reflections of the HADES-URF are clearly visible (orange marker) at 220 ms.</i>	<i>60</i>
<u>Figure 3-35:</u>	<i>Indication of the main faults on seismic line 8417. The position of the line is shown in Figure 3-26.....</i>	<i>61</i>
<u>Figure 3-36:</u>	<i>Regional network of piezometric measurements of SCK•CEN (S) and available piezometers of the Geological Survey of Belgium (P).</i>	<i>62</i>
<u>Figure 3-37:</u>	<i>(a) Piezometric changes in some piezometers typical of the Miocene Aquifer (Diest Sand). (b) Piezometric change in some piezometers typical of the Lower-Rupelian Aquifer; (c) Piezometric changes in some piezometers typical of the Lede-Brussel Aquifer (for the exact location of the observation points see Figure 3-36).</i>	<i>63</i>
<u>Figure 3-38:</u>	<i>(a) Piezometric change in different aquifers measured at Herentals (ground level = 17.7 mTAW); (b) Piezometric change in different aquifers measured on the Mol site (ground level = 24.4 mTAW).</i>	<i>64</i>
<u>Figure 3-39:</u>	<i>(a) Piezometric map of the Pliocene Aquifer based on measurements in December 1990; (b) Piezometric map of the Miocene Aquifer based on measurements in December 1990.....</i>	<i>65</i>

<u>Figure 3-40:</u>	<i>(a) Piezometric map of the Lower-Rupelian Aquifer based on measurements in December 1993; (b) Piezometric map of the Lede-Brussel Aquifer based on measurements in December 1993.</i>	66
<u>Figure 3-41:</u>	<i>Schematic of hydrogeological units and flows in an east-west section through Mol.</i>	67
<u>Figure 3-42:</u>	<i>Chemical composition of the groundwaters of (a) the Pliocene Aquifer (b) the Diest Sand of the Miocene Aquifer (c) the Berchem Sand of the Miocene Aquifer (d) the Lower-Rupelian Aquifer (e) Lede-Brussel Aquifer (f) the Maastricht and Landen Aquifers [56].....</i>	68
<u>Figure 3-43:</u>	<i>Change in total dissolved salts (TDS) in the Lower-Rupelian Aquifer as a function of depth, showing two straight trend lines (I and II), according to [56]; For the exact location of the observation points see Figure 3-36 (18: Kontich; 41: Oelegem; 19: Wuustwezel; 20: Meer; 1: Mol (SCK•CEN); 16: Balen; 14: Lommel).</i>	69
<u>Figure 3-44:</u>	<i>Age of waters in the Lower-Rupelian Aquifer (years), corrected according to the Pearson model in [56] (See Figure 3-49 for the areal extent and the grid of the hydrogeological model used).</i>	69
<u>Figure 3-45:</u>	<i>CMR curve and hydraulic conductivity measurements on samples from the Boom Clay in the Mol-1 borehole. Kh: horizontal hydraulic conductivity; Kv: vertical hydraulic conductivity; K-Mig: hydraulic conductivity determined from migration tests with tritiated water (HTO) and iodine (I).</i>	70
<u>Figure 3-46:</u>	<i>Distribution of hydraulic conductivities determined on cores from the Mol-1 borehole based on migration experiments using tritiated water (Kv-MIG-HTO) and iodine-131 (Kv-MIG-I-131), or based on conventional tests on small cylinders or plugs, cut vertically and parallel to the bedding, in permeameters (Kv-Hyd, Kh-Hyd) [125].</i>	71

<u>Figure 3-47:</u>	<i>Laboratory estimates and measurements of vertical hydraulic conductivity. An estimate is made from the correlation between certain components of the granulometry and hydraulic conductivity according to whether the correlation relates to the Boom Clay only (Kv estim GrSize BC) or to the whole of the cored profile (Kv estim GrSize profile). Another way of estimating K is to analyse and calibrate magnetic resonance data (Kv estim CMR).</i>	72
<u>Figure 3-48:</u>	<i>The aeral extent and distribution of the hydrogeological units in the regional, sub-regional and local groundwater flow models.</i>	73
<u>Figure 3-49:</u>	<i>Grid network of the 1984 regional model [130].</i>	74
<u>Figure 3-50:</u>	<i>Area of the 1994 regional model and extent of the different hydrogeological units [49].</i>	75
<u>Figure 3-51:</u>	<i>Grids for the different aquifer units of regional model NEB94 and their boundary conditions a) Quaternary, b) Pliocene, c) Miocene, d) Lower-Rupelian and e) Lede-Brussel [49].</i>	76
<u>Figure 3-52:</u>	<i>Calculated hydraulic heads for the Neogene Aquifers using the basic version of the regional model (NEB06N) [49].</i>	77
<u>Figure 3-53:</u>	<i>Hydraulic heads calculated using the basic version of the regional model (NEB06N) [49], a) Lower-Rupelian b) Lede-Brussel.</i>	78
<u>Figure 3-54:</u>	<i>Rate of groundwater flow (>0: ascending, <0: descending) through the Boom Clay for the reference version of the regional model (NEB06N: considering a K' for the Boom Clay of $3 \cdot 10^{-12}$ m/s), expressed in 10^{-3} mm/year [49].</i>	79
<u>Figure 3-55:</u>	<i>Flow rate(>0: ascending, <0: descending) through the Boom Clay for the version that allows for faults (Z1+Z2) and a greater permeability of the Boom Clay (NEB06F3: K of the Boom Clay of $3 \cdot 10^{-10}$ m/s), expressed in 10^{-3} mm/year [49].</i>	80
<u>Figure 3-56:</u>	<i>Hydraulic head distribution in the Lower-Rupelian Aquifer with the version of the regional model where a higher transmissivity of the Lower-Rupelian Aquifer has been taken into account [49].</i>	81

<u>Figure 3-57:</u>	<i>SCK•CEN's regional piezometric network K and the zones for further exploratory drilling recommended in 1994.....</i>	82
<u>Figure 3-58:</u>	<i>Impact of a reduction in infiltration by a factor of 3 on the distribution of hydraulic heads in the Neogene (a: reference; b: modification) and the Lower-Rupelian (c: reference d: modification) according to [130].</i>	83
<u>Figure 3-59:</u>	<i>Impact of fluvial erosion due to a drop in sea level on the distribution of hydraulic heads in the Neogene (a: reference; b: modification) and the Lower-Rupelian (c: reference d: modification) according to [130].</i>	84
<u>Figure 3-60:</u>	<i>Hydraulic heads in the Quaternary and Pliocene Aquifer calculated with a reduction in infiltration of 50% compared to the present-day infiltration [145].</i>	85
<u>Figure 3-61:</u>	<i>Contours of hydraulic head calculated using the sub-regional model.</i>	86
<u>Figure 3-62:</u>	<i>Particle trackings from the base of the Berchem Sands at the Mol-Dessel nuclear zone, calculated using the sub-regional model [150].</i>	87
<u>Figure 3-63:</u>	<i>Chronostratigraphic and lithostratigraphic position of the Ypresian Clays.</i>	88
<u>Figure 3-64:</u>	<i>Correlation of the lithostratigraphic subdivisions of the Ypresian (modified according to [155]).</i>	89
<u>Figure 3-65:</u>	<i>Isopachs and depth to top of the Kortrijk Formation [156].</i>	90
<u>Figure 3-66:</u>	<i>Overview of the hydrographic network in northwest Flanders showing falls (hydraulic gradients) and catchment areas.</i>	91
<u>Figure 3-67:</u>	<i>Stratigraphic east-west section through northern Belgium through the Kortrijk Formation investigation area [23].</i>	92
<u>Figure 3-68:</u>	<i>Elevation variations in mm between 1948 and 1980 with the Uccle geodetic point as reference, and the fault pattern in the Brabant Massif [38, 159]. The investigation area for the Ypresian Clays is shown in colour.</i>	93
<u>Figure 3-69:</u>	<i>Fault pattern in the Kortrijk Formation at Marke.</i>	94
<u>Figure 3-70:</u>	<i>Geothermal potential and mineral resources in northwest Flanders.</i>	95

<u>Figure 3-71:</u>	<i>Hydrogeological environment of the investigation area on a vertical section through Knokke-Assenede-Kallo: vertical groundwater flow under natural conditions (a) and in the present situation with groundwater extraction (b) [23].</i>	96
<u>Figure 3-72:</u>	<i>Detailed lithological and hydrogeological structure in the centre of the investigation area [160].</i>	97
<u>Figure 3-73:</u>	<i>Position of the Doel boreholes.</i>	98
<u>Figure 3-74:</u>	<i>Stratigraphic interpretation, wireline logging intervals, the location of pulse tests and the cored intervals for the boreholes at Doel.</i>	99
<u>Figure 3-75:</u>	<i>Distribution of carbonate, organic material and iron contents and the fraction greater than 50μm in the cored section of Ypresian Clays from borehole Doel-1A. Ko: Kortemark Member; Al: Aalbeke Member.</i>	100
<u>Figure 3-76:</u>	<i>Distribution of carbonate, feldspar and quartz contents in the silt fraction of the Ypresian Clays. Ko: Kortemark Member; Al: Aalbeke Member.</i>	101
<u>Figure 3-77:</u>	<i>Clay mineralogy of the clay fraction of the Ypresian Clay. Ko: Kortemark Member; Al: Aalbeke Member.</i>	102
<u>Figure 3-78:</u>	<i>Clay mineralogy of the silt fraction of the Ypresian Clay. Ko: Kortemark Member; Al: Aalbeke Member.</i>	103
<u>Figure 3-79:</u>	<i>Hydraulic heads measured in piezometers at Doel in formations from Neogene age to Palaeozoic age.</i>	104
<u>Figure 3-80:</u>	<i>Hydraulic conductivity (K), apparent diffusion coefficient (D_{app}) and the product ηR (porosity available for diffusion multiplied by the retardation factor) for the Ypresian Clays. GR: gamma ray log.</i>	105
 Chapter 4		
<u>Figure 4-1:</u>	<i>General view of the deep disposal facility for vitrified waste (reference repository design).</i>	107
<u>Figure 4-2:</u>	<i>Section through a disposal gallery for vitrified waste (reference repository design).</i>	107
<u>Figure 4-3:</u>	<i>Configuration for the calculation of maximum temperatures around a disposal gallery.</i>	108

<u>Figure 4-4:</u>	<i>Maximum temperatures around a disposal gallery – temperature profile as a function of thermal conductivity of backfill material.</i>	<i>108</i>
<u>Figure 4-5:</u>	<i>Rate of transformation from smectite to illite.</i>	<i>109</i>
<u>Figure 4-6:</u>	<i>The HADES design – SAFIR (1989).</i>	<i>109</i>
<u>Figure 4-7:</u>	<i>The Belgian design– SAFIR (1989).</i>	<i>109</i>
<u>Figure 4-8:</u>	<i>General view of a repository design for spent fuel elements.</i>	<i>110</i>
<u>Figure 4-9:</u>	<i>Section through a disposal gallery for spent fuel elements. ...</i>	<i>110</i>
<u>Figure 4-10:</u>	<i>OPHELIE mock-up: linear and transverse section.</i>	<i>110</i>
<u>Figure 4-11:</u>	<i>View of the OPHELIE mock-up: instrumentation.</i>	<i>111</i>
<u>Figure 4-12:</u>	<i>General view of the OPHELIE mock-up.</i>	<i>112</i>
<u>Figure 4-13:</u>	<i>OPHELIE mock-up: backfill blocks.</i>	<i>112</i>

Chapter 5

<u>Figure 5-1:</u>	<i>The HADES Underground Research Facility beneath the SCK•CEN site.</i>	<i>113</i>
<u>Figure 5-2:</u>	<i>Simplified SW-NE geological section beneath the Mol-Dessel nuclear zone with indication of the approximate position of the second shaft. The dip of the formations is about 1-2%.</i>	<i>113</i>
<u>Figure 5-3:</u>	<i>Mechanical analogy of various geomechanical models used to describe the Boom Clay behaviour (from top to bottom: elasto-plastic model, elasto-visco-plastic model, elasto-visco-plastic model modified by addition of a short-term threshold and formulation in effective stresses).</i>	<i>114</i>
<u>Figure 5-4:</u>	<i>Evolution of the diametrical convergence of the lining of the Test Drift as a function of time since the installation of various concrete block rings.</i>	<i>114</i>
<u>Figure 5-5:</u>	<i>Layout of the underground facility (HADES-URF) as existing in 1987. The experimental gallery (also called ‘laboratory’) was excavated in frozen clay, while the experimental shaft and drift as well as the Test Drift were excavated without freezing.</i>	<i>115</i>
<u>Figure 5-6:</u>	<i>Emplacement scheme for the multi-layer lining of the first shaft (outer layer of concrete, polyethylene membrane, inner layer of concrete).</i>	<i>115</i>

<u>Figure 5-7:</u>	<i>View of the top of the freezing tubes (approximately 250 m depth) around the location of the first shaft.....</i>	<i>116</i>
<u>Figure 5-8:</u>	<i>Passage of a measuring instrument through the watertight polythene membrane used in the lining of the first shaft.</i>	<i>116</i>
<u>Figure 5-9:</u>	<i>Lay-out of the two successive series of freezing tubes used for the excavation of the HADES experimental gallery.</i>	<i>117</i>
<u>Figure 5-10:</u>	<i>HADES experimental gallery: view of the lining made of nodular cast iron segments and of one of the access to the clay massif (on the left).</i>	<i>117</i>
<u>Figure 5-11:</u>	<i>Headframe of the first shaft of the HADES-URF.....</i>	<i>118</i>
<u>Figure 5-12:</u>	<i>Scheme of the small shaft and gallery of the HADES-URF with indication of the emplaced geomechanical instrumentation.</i>	<i>119</i>
<u>Figure 5-13:</u>	<i>Test Drift excavation scheme.</i>	<i>119</i>
<u>Figure 5-14:</u>	<i>View of the excavation face of the Test Drift while emplacing the 60 cm thick concrete block lining.</i>	<i>120</i>
<u>Figure 5-15:</u>	<i>Test Drift: view of the lining made out of sliding steel ribs.</i>	<i>120</i>
<u>Figure 5-16:</u>	<i>'As built' plan of the second shaft showing the foundation in the top part of the Boom Clay as well as the two starting chambers.....</i>	<i>121</i>
<u>Figure 5-17:</u>	<i>Second shaft: excavation in the frozen sands (jackhammer mounted on an hydraulic arm and manual air hammers).</i>	<i>122</i>
<u>Figure 5-18:</u>	<i>Second shaft: guniting of the outer lining (20 cm of shotcrete on reinforcing mats).</i>	<i>122</i>
<u>Figure 5-19:</u>	<i>Second shaft: scheme of the excavation of the foundation.....</i>	<i>123</i>
<u>Figure 5-20:</u>	<i>Second shaft: prefabricated section of the inner lining in the headframe waiting to be lifted onto the service platform prior to descent.....</i>	<i>124</i>
<u>Figure 5-21:</u>	<i>Second shaft: excavation method (hydraulic arm) and support (sliding ribs) below the foundation.</i>	<i>125</i>
<u>Figure 5-22:</u>	<i>Second shaft: service platform and support of sliding ribs (looking upwards).</i>	<i>125</i>
<u>Figure 5-23:</u>	<i>Second shaft: placement of reinforcement for the starting chambers.</i>	<i>126</i>
<u>Figure 5-24:</u>	<i>Second shaft: excavation of the starting chambers.....</i>	<i>126</i>

<u>Figure 5-25:</u>	<i>Second shaft: slip planes and fractures observed during excavation of the starting chambers. The upper picture shows a fallen block in the south starting chamber due to a circular (vis-à-vis the centre of the second shaft) slip plane. The below picture shows the side wall of the same starting chamber displaying cross-sections of two of the encountered fractures (average dip was 35° towards the centre of the shaft).....</i>	<i>127</i>
<u>Figure 5-26:</u>	<i>Principle of the expended segmental lining consisting of rings of unreinforced concrete segments plus 1 or 2 'wedge blocks' (or key) per ring. The wedge blocks are used to ensure close contact with the rock mass.....</i>	<i>128</i>
<u>Figure 5-27:</u>	<i>Scheme of the HADES-URF (2000 situation) indicating the location of the CLIPEX instrumentation boreholes on both ends of the planned connecting gallery.</i>	<i>128</i>
<u>Figure 5-28:</u>	<i>Alternative repository designs for spent fuel disposal based on the possibility to excavate large cavities in the Boom Clay.....</i>	<i>129</i>
<u>Figure 5-29:</u>	<i>Principle of the Cam-clay model.</i>	<i>130</i>
<u>Figure 5-30:</u>	<i>Results of the modelling (interstitial pressures, radial stresses, radial displacements) of the excavation of the connecting gallery with the Cam-clay model.....</i>	<i>130</i>
<u>Figure 5-31:</u>	<i>PRACLAY: contours of equal temperatures after 3 years of heating (3D Mohr-Coulomb model).</i>	<i>131</i>
<u>Figure 5-32:</u>	<i>PRACLAY: contours of equal interstitial pressures after 3 years of heating (3D Mohr-Coulomb model).....</i>	<i>131</i>
<u>Figure 5-33:</u>	<i>Principle of the expandable lining for the microtunneller.....</i>	<i>132</i>

Chapter 6

<u>Figure 6-1:</u>	<i>Overpack used for primary packages of SYNATOM vitrified waste (shown without trolleys).....</i>	<i>133</i>
<u>Figure 6-2:</u>	<i>Overpack for SYNATOM vitrified waste.....</i>	<i>134</i>
<u>Figure 6-3:</u>	<i>Transfer wagon.</i>	<i>135</i>
<u>Figure 6-4:</u>	<i>Pushing robot pushing an overpack.....</i>	<i>136</i>
<u>Figure 6-5:</u>	<i>Transfer wagon (PRACLAY demonstration hall).</i>	<i>136</i>
<u>Figure 6-6:</u>	<i>Transfer wagon (PRACLAY demonstration hall).</i>	<i>137</i>
<u>Figure 6-7:</u>	<i>Transfer wagon (PRACLAY demonstration hall).</i>	<i>137</i>

<u>Figure 6-8:</u>	<i>'Bottles' for spent fuel.....</i>	<i>138</i>
Chapter 7		
--		
Chapter 8		
--		
Chapter 9		
<u>Figure 9-1:</u>	<i>Experimental setup of the RESEAL demonstration test.</i>	<i>139</i>
Chapter 10		
--		
Chapter 11		
<u>Figure 11.2-1:</u>	<i>Role of the safety assessment in the stepwise process of developing and implementing a disposal system (SA stands for safety assessment).....</i>	<i>141</i>
<u>Figure 11.2-2:</u>	<i>The role of the safety assessment in the stepwise decision process [1].</i>	<i>142</i>
<u>Figure 11.2-3:</u>	<i>Schematic presentation of the successive steps in long-term safety assessments.....</i>	<i>143</i>
<u>Figure 11.2-4:</u>	<i>The various successive steps of scenario development.....</i>	<i>143</i>
<u>Figure 11.2-5:</u>	<i>Main components of the disposal system and its environment.....</i>	<i>144</i>
<u>Figure 11.3.1-1:</u>	<i>Area of the repository site considered in the safety assessments.</i>	<i>145</i>
<u>Figure 11.3.1-2:</u>	<i>General scheme for the disposal of category B waste and high-level vitrified waste (ZAGALC) in a single repository. ...</i>	<i>145</i>
<u>Figure 11.3.1-3:</u>	<i>Cross section of a disposal gallery for high-level vitrified waste (ZAGALC).</i>	<i>146</i>
<u>Figure 11.3.1-4:</u>	<i>Cross section of a disposal gallery for uranium oxide spent fuel (ZAGALS).</i>	<i>146</i>

<u>Figure 11.3.1-5:</u>	<i>Cross section of a disposal gallery for MOX spent fuel (ZAGALS).....</i>	<i>147</i>
<u>Figure 11.3.1-6:</u>	<i>Plan view of the configuration of disposal galleries and main galleries for spent fuel (ZAGALS).....</i>	<i>147</i>
<u>Figure 11.3.1-7:</u>	<i>Considered configuration for the poor-sealing scenario (see Section 11.5.4) for spent fuel (ZAGALS).</i>	<i>148</i>
<u>Figure 11.3.1-8:</u>	<i>Cross section of a disposal gallery for hulls and endpieces (HAGALC2).</i>	<i>148</i>
<u>Figure 11.3.1-9:</u>	<i>Vertical profile of the hydraulic and migration parameters in the Boom Clay (Mol-1 borehole).</i>	<i>149</i>
<u>Figure 11.3.1-10:</u>	<i>Extent of the different hydrogeological models.</i>	<i>150</i>
<u>Figure 11.3.3-1:</u>	<i>Polarisation curve, with E the potential (in mV) and I the current density (in A).</i>	<i>151</i>
<u>Figure 11.3.4-1:</u>	<i>Principal stages of corrosion (flowchart) (from [4]).....</i>	<i>153</i>
<u>Figure 11.3.4-2:</u>	<i>Evolution in the kinetics of the dissolution reaction of glass over time (generic case) (from [6]).</i>	<i>153</i>
<u>Figure 11.3.4-3:</u>	<i>Dissolution behaviour of SYNATOM R7T7 glass in different media at 90°C.....</i>	<i>154</i>
<u>Figure 11.3.4-4:</u>	<i>Dissolution behaviour of different types of glass (in situ tests at 90°C).....</i>	<i>154</i>
<u>Figure 11.3.4-5:</u>	<i>SIMS analysis profiles for SYNATOM R7T7 and SAN60 glasses (in situ tests over 3.5 years at 90°C).</i>	<i>155</i>
<u>Figure 11.3.4-6:</u>	<i>Configurations used to model the water/glass/clay system. ...</i>	<i>155</i>
<u>Figure 11.3.4-7:</u>	<i>Comparison between experimental data and theoretical predictions for the SYNATOM R7T7 glass (tests conducted at 90°C).</i>	<i>156</i>
<u>Figure 11.3.4-8:</u>	<i>Evolution of the physical characteristics of EUROBITUM matrices with time.</i>	<i>156</i>
<u>Figure 11.3.4-9:</u>	<i>Influence of the pressure on the swelling of bituminised waste (tests conducted at 23°C).</i>	<i>157</i>
<u>Figure 11.3.4-10:</u>	<i>Influence of the temperature on the swelling of bituminised waste (P = 0.1 MPa).</i>	<i>157</i>
<u>Figure 11.3.4-11:</u>	<i>Evolution of the alpha activity of spent fuels over time.</i>	<i>158</i>
<u>Figure 11.3.6-1:</u>	<i>Contours of interstitial pressure calculated in the plane Z = -229 m after 10.5 years of excavation of the HADES Underground Research Facility.....</i>	<i>159</i>

<u>Figure 11.3.6-2:</u>	<i>Measurements of hydraulic conductivity carried out from the HADES URF.</i>	159
<u>Figure 11.3.6-3:</u>	<i>Schematic of the CERBERUS experiment.....</i>	160
<u>Figure 11.3.6-4:</u>	<i>Hydraulic conductivity as a function of the breakthrough pressure [44].....</i>	160
<u>Figure 11.3.6-5:</u>	<i>Schematic setup of the isostatic experiments [35].....</i>	161
<u>Figure 11.3.6-6:</u>	<i>Illustration of non-Darcian behaviour (variation in the gas flow rate when preferential pathways have been formed) [35].....</i>	162
<u>Figure 11.3.6-7:</u>	<i>Setup of filters for the in situ gas injection experiments.....</i>	162
<u>Figure 11.3.6-8:</u>	<i>Pressure curve (MPa) in filters 18, 19 and 21 following a gas injection in filter 20 (for the filter positions see Figure 11.3.6-7).....</i>	163
<u>Figure 11.3.6-9:</u>	<i>Pressure curve (MPa) in filter 12 following a gas injection in filter 20 (for the filter positions see Figure 11.3.6-7).....</i>	163
<u>Figure 11.3.6-10:</u>	<i>Variation in gas flow rate between filters 13 and 14 due to the opening and closing of the preferential gas pathways (for the filter positions see Figure 11.3.6-7).....</i>	164
<u>Figure 11.3.6-11:</u>	<i>Change in tritium activity in filters 12, 13 and 14 after injection of tritium in filter 13 (for the filter positions see Figure 11.3.6-7).....</i>	164
<u>Figure 11.3.7-1:</u>	<i>General overview of the temperatures (°C) attained at different time steps around a repository for vitrified high-level ZAGALC waste.....</i>	165
<u>Figure 11.3.7-2:</u>	<i>Increase of the attained temperature (K) between 100 and 300 years after disposal of vitrified high-level ZAGALC waste into an underground waste repository in the Boom Clay.....</i>	166
<u>Figure 11.3.7-3:</u>	<i>Increase of maximal attained temperature (K) around the vitrified high-level ZAGALC waste disposed in an underground repository in function of the thermal conductivity of the backfill material.....</i>	166
<u>Figure 11.3.7-4:</u>	<i>Configuration for the calculations in [10].....</i>	167
<u>Figure 11.3.7-5:</u>	<i>Temperature increase (K) in the near field resulting from the disposal in a 'single-seater' design of spent fuel with a burn-up of 36 GWd/tHM and taking a precooling time of 60 years into account.....</i>	167

<u>Figure 11.3.8-1:</u>	<i>Schematic representation of interactions possibly involved with organic matter which can influence the migration behaviour of the radionuclides.</i>	169
<u>Figure 11.3.8-2:</u>	<i>Schematic representation of diffusion test.</i>	169
<u>Figure 11.3.8-3:</u>	<i>Schematic representation of percolation test.</i>	169
<u>Figure 11.3.8-4:</u>	<i>In situ test for HTO (CPI): comparison between experimental results and theoretical predictions.</i>	170
<u>Figure 11.3.8-5:</u>	<i>Variation in ηRD_{app} as a function of the consolidation pressure for different non-sorbed species.</i>	171
<u>Figure 11.3.8-6:</u>	<i>Variation in ηRD_{app} as a function of ηR for different non-sorbed species.</i>	171
<u>Figure 11.3.8-7:</u>	<i>In situ test with Γ: comparison between experimental results and theoretical predictions (vertical piezometer).</i>	172
<u>Figure 11.3.8-8:</u>	<i>In situ test with Γ: comparison between experimental results and theoretical predictions (horizontal piezometer).</i>	172
<u>Figure 11.3.8-9:</u>	<i>In situ percolation test with Cs: activity profile of ^{134}Cs in the clay core.</i>	173
<u>Figure 11.3.8-10:</u>	<i>Reactional scheme applied for the ^{14}C labelling of organic matter.</i>	174
<u>Figure 11.3.8-11:</u>	<i>Elution profiles of ^{14}C labelled organic matter as a function of the molecular fraction.</i>	174
<u>Figure 11.3.8-12:</u>	<i>Examples of mechanisms capable of inhibiting the migration of colloids in a porous medium.</i>	175
<u>Figure 11.3.8-13:</u>	<i>Characterisation of the organic matter: comparison between test results obtained by titration (DET) and theoretical predictions (modelling with 3 sites).</i>	176
<u>Figure 11.3.8-14:</u>	<i>Abundance of carbonate and organic complexes (humic acids) of americium in Boom Clay as a function of pH.</i>	176
<u>Figure 11.3.8-15:</u>	<i>Americium masked by organic matter.</i>	177
<u>Figure 11.3.8-16:</u>	<i>Mol I borehole: migration tests with HTO and Γ.</i>	177
<u>Figure 11.3.8-17:</u>	<i>Radionuclides concentrations in the percolation solutions as a function of time.</i>	178
<u>Figure 11.3.9-1:</u>	<i>Delimitation of the different modelled zones.</i>	179
<u>Figure 11.3.9-2:</u>	<i>Extent of the local model.</i>	179

<u>Figure 11.3.9-3:</u>	<i>Calculated head distribution for the third layer of the local model.....</i>	<i>180</i>
<u>Figure 11.3.9-4:</u>	<i>Particle trackings from the base of the Berchem Sands at the Mol-Dessel nuclear zone, calculated using the local model.....</i>	<i>180</i>
<u>Figure 11.3.10-1:</u>	<i>Biosphere receptors for the Mol-Dessel reference site.....</i>	<i>181</i>
<u>Figure 11.3.10-2:</u>	<i>Exposure pathways for the Mol-Dessel reference site.....</i>	<i>181</i>
<u>Figure 11.5.2-1:</u>	<i>Schematic overview of the processes that are considered in the normal evolution scenario for each of the components of the disposal system and the environment.</i>	<i>183</i>
<u>Figure 11.5.2-2:</u>	<i>Robustness of the main components of the disposal system and its environment.....</i>	<i>184</i>
<u>Figure 11.5.3-1:</u>	<i>Considered configuration and simplifications for migration calculations through the near field and the Boom Clay.</i>	<i>185</i>
<u>Figure 11.5.3-2:</u>	<i>Schematic of the two-dimensional grid used for migration calculations through the near field and the clay layer for disposal of the high-level vitrified waste (ZAGALC).....</i>	<i>185</i>
<u>Figure 11.5.3-3:</u>	<i>Activity flux to the overlying aquifer for ¹²⁹I with ZAGALC waste.....</i>	<i>186</i>
<u>Figure 11.5.3-4:</u>	<i>Activity flux to the overlying aquifer for activation and fission products with ZAGALC waste.</i>	<i>186</i>
<u>Figure 11.5.3-5:</u>	<i>Activity flux to the overlying aquifer for actinides from the 4N chain with ZAGALC waste.</i>	<i>187</i>
<u>Figure 11.5.3-6:</u>	<i>Activity flux to the overlying aquifer for actinides from the 4N+1 chain with ZAGALC waste.....</i>	<i>187</i>
<u>Figure 11.5.3-7:</u>	<i>Activity flux to the overlying aquifer for actinides from the 4N+2 chain with ZAGALC waste.....</i>	<i>188</i>
<u>Figure 11.5.3-8:</u>	<i>Activity flux to the overlying aquifer for actinides from the 4N+3 chain with ZAGALC waste.....</i>	<i>188</i>
<u>Figure 11.5.3-9:</u>	<i>Activity flux to the overlying aquifer for ²⁴²Pu from the 4N+2 chain with ZAGALC waste.....</i>	<i>189</i>
<u>Figure 11.5.3-10:</u>	<i>Activity flux to the overlying aquifer for three different boundary conditions with HAGALC2 waste.....</i>	<i>189</i>
<u>Figure 11.5.3-11:</u>	<i>Activity flux to the overlying aquifer for activation and fission products with HAGALC2 waste.....</i>	<i>190</i>

<u>Figure 11.5.3-12:</u>	<i>Activity flux to the overlying aquifer for actinides from the 4N chain with HAGALC2 waste.....</i>	<i>190</i>
<u>Figure 11.5.3-13:</u>	<i>Activity flux to the overlying aquifer for actinides from the 4N+1 chain with HAGALC2 waste.....</i>	<i>191</i>
<u>Figure 11.5.3-14:</u>	<i>Activity flux to the overlying aquifer for actinides from the 4N+2 chain with HAGALC2 waste.....</i>	<i>191</i>
<u>Figure 11.5.3-15:</u>	<i>Activity flux to the overlying aquifer for actinides from the 4N+3 chain with HAGALC2 waste.....</i>	<i>192</i>
<u>Figure 11.5.3-16:</u>	<i>Activity flux to the overlying aquifer for ²⁴²Pu from the 4N+2 chain with HAGALC2 waste.....</i>	<i>192</i>
<u>Figure 11.5.3-17:</u>	<i>Evolution of the corroded fraction of the spent fuel matrix; comparison between the SPA source term model and the α auto-oxidation model for the spent fuel types considered (with or without a minimum rate of corrosion). The life of the overpack is assumed to be 2000 years.</i>	<i>193</i>
<u>Figure 11.5.3-18:</u>	<i>Grid used for the migration calculations through the near field and clay layer with ZAGALS waste.</i>	<i>194</i>
<u>Figure 11.5.3-19:</u>	<i>Coarser discretisation used for migration calculations through the near field and the clay layer with ZAGALS waste.....</i>	<i>194</i>
<u>Figure 11.5.3-20:</u>	<i>Comparison of the ¹⁰⁷Pd concentration contours for a fine and a coarse discretisation. ¹⁰⁷Pd attains its solubility limit (40 700 Bq/m³) in the source.</i>	<i>195</i>
<u>Figure 11.5.3-21:</u>	<i>Evolution of the fluxes for activation and fission products for the SPA source term.</i>	<i>195</i>
<u>Figure 11.5.3-22:</u>	<i>Evolution of the fluxes for activation and fission products for the α auto-oxidation model.</i>	<i>196</i>
<u>Figure 11.5.3-23:</u>	<i>Evolution of the fluxes for actinides for α auto-oxidation source term (Data set 2).....</i>	<i>196</i>
<u>Figure 11.5.3-24:</u>	<i>Evolution of the fluxes for actinides for α auto-oxidation source term (Data set 2').</i>	<i>197</i>
<u>Figure 11.5.3-25:</u>	<i>Distribution of the radionuclide concentration (Bq/m³) in the water of the Berchem Sands for a radionuclide flux of 1 MBq/year from the Boom Clay.</i>	<i>197</i>
<u>Figure 11.5.3-26:</u>	<i>Distribution of the radionuclide concentration (Bq/m³) in the water of the Diest Sands for a radionuclide flux of 1 MBq/year from the Boom Clay.</i>	<i>198</i>

<u>Figure 11.5.3-27:</u>	<i>Distribution of the radionuclide concentration (Bq/m³) in the water of the Mol Sands for a radionuclide flux of 1 MBq/year from the Boom Clay.</i>	198
<u>Figure 11.5.3-28:</u>	<i>Impact of the hydraulic gradients over the Boom Clay on the radionuclide flux through the clay layer/aquifer interface.</i>	199
<u>Figure 11.5.3-29:</u>	<i>Impact of the hydraulic gradients over the Boom Clay on the radionuclide concentrations in the aquifer.</i>	199
<u>Figure 11.5.3-30:</u>	<i>Evolution in the total dose rate via a well with ZAGALC waste.</i>	200
<u>Figure 11.5.3-31:</u>	<i>Contributions by the various actinides to the dose rate via a well with ZAGALC waste.</i>	200
<u>Figure 11.5.3-32:</u>	<i>Evolution in the total dose rate via the river pathway for ZAGALC waste.</i>	201
<u>Figure 11.5.3-33:</u>	<i>Evolution of the total dose rate via a well with HAGALC2 waste.</i>	201
<u>Figure 11.5.3-34:</u>	<i>Evolution of the total dose rate via the river pathway with HAGALC2 waste.</i>	202
<u>Figure 11.5.3-35:</u>	<i>Evolution in the dose rate via the well pathway for the fission and activation products (1980 tonnes of spent uranium oxide fuel with a burn-up fraction of 55 GWd/tHM).</i>	202
<u>Figure 11.5.3-36:</u>	<i>Evolution in the dose rate via the well pathway for actinides (Data set 2, 1980 tonnes of spent uranium oxide fuel with a burn-up of 55 GWd/tHM).</i>	203
<u>Figure 11.5.3-37:</u>	<i>Evolution in the dose rate via the well pathway for actinides (Data set 2', 1980 tonnes of spent uranium oxide fuel with a burn-up of 55 GWd/tHM).</i>	203
<u>Figure 11.5.3-38:</u>	<i>Evolution in the total dose rate of the three fuel types considered (with Data set 2 for the actinides) for a well in the Sands of Diest.</i>	204
<u>Figure 11.5.3-39:</u>	<i>Evolution in the total dose rate via the river pathway for the three fuel types considered (with Data set 2 for the actinides).</i>	204
<u>Figure 11.5.3-40:</u>	<i>Evolution in the dose rate via a well for the activation and fission products for two different half-lives of ⁷⁹Se (spent uranium oxide fuel with a burn-up of 55 GWd/tHM).</i>	205

<u>Figure 11.5.3-41:</u>	<i>Evolution in the dose rate for the two reprocessing options considered.</i>	205
<u>Figure 11.5.3-42:</u>	<i>Cumulative activity that reaches the aquifers (ZAGALC). The calculation of this activity makes no allowance for radioactive decay in the aquifers.</i>	206
<u>Figure 11.5.3-43:</u>	<i>Flowchart of the LISA code.</i>	206
<u>Figure 11.5.3-44:</u>	<i>Evolution in the expectation value and percentiles for ZAGALC waste for the simplified normal-evolution scenario.</i>	207
<u>Figure 11.5.3-45:</u>	<i>Evolution in the expectation value and percentiles for ZAGALC waste for the normal-evolution scenario.</i>	207
<u>Figure 11.5.3-46:</u>	<i>Evolution in the expectation value and percentiles for hulls and endpieces for the simplified normal-evolution scenario.</i>	208
<u>Figure 11.5.3-47:</u>	<i>Evolution in the partial rank correlation coefficients calculated for high-level vitrified waste in the case of a simplified normal-evolution scenario, part I.</i>	208
<u>Figure 11.5.3-48:</u>	<i>Evolution in the partial rank correlation coefficients calculated for high-level vitrified waste in the case of a simplified normal-evolution scenario, part II.</i>	209
<u>Figure 11.5.3-49:</u>	<i>Evolution in the partial rank correlation coefficients calculated for high-level vitrified waste in the case of a simplified normal-evolution scenario, part III.</i>	209
<u>Figure 11.5.3-50:</u>	<i>Flowchart of the stochastic calculations.</i>	210
<u>Figure 11.5.3-51:</u>	<i>Evolution in the expectation value and percentiles for spent fuel (1980 tonnes of spent uranium oxide fuel with a burn-up of 55 GWd/tHM).</i>	210
<u>Figure 11.5.3-52:</u>	<i>Evolution in the partial rank correlation coefficients calculated for spent fuel (1980 tonnes of spent uranium oxide fuel with a burn-up of 55 GWd/tHM).</i>	211
<u>Figure 11.5.4-1:</u>	<i>Schematic representation of the ‘exploitation drilling’ scenario.</i>	213
<u>Figure 11.5.4-2:</u>	<i>Calculated concentration distribution of ¹²⁹I after 200 000 years in the case of exploitation drilling.</i>	213
<u>Figure 11.5.4-3:</u>	<i>Simplified two-dimensional section through the disposal system.</i>	214
<u>Figure 11.5.4-4:</u>	<i>More realistic geometry for the influx of groundwater to the gallery.</i>	214

<u>Figure 11.5.4-5:</u>	<i>Concentration distribution in the aquifer due to poor sealing.</i>	215
<u>Figure 11.5.4-6:</u>	<i>Flux of ^{237}Np from the Boom Clay into the aquifer due to poor sealing.</i>	215
<u>Figure 11.5.4-7:</u>	<i>Evolution of the ^{129}I dose rate for 1980 tHM fuel with a burn-up of 55 GWd/tHM in the case of poor sealing.</i>	216
<u>Figure 11.5.4-8:</u>	<i>Cumulative hydrogen production due to the disposal of vitrified high-level waste (ZAGALC).</i>	216
<u>Figure 11.5.4-9:</u>	<i>Cumulative methane production due to the disposal of vitrified high-level waste (ZAGALC).</i>	217
<u>Figure 11.5.4-10:</u>	<i>Cumulative hydrogen production due to the disposal of spent fuel assemblies (ZAGALS).</i>	217
<u>Figure 11.5.4-11:</u>	<i>Cumulative methane production due to the disposal of spent fuel assemblies (ZAGALS).</i>	218
<u>Figure 11.5.4-12:</u>	<i>Cumulative methane production for Eurobitumen packed in carbon steel drums (MAGALE).</i>	218
<u>Figure 11.5.4-13:</u>	<i>Calculated flux of ^{129}I from the Boom Clay to the Neogene Aquifer for the normal-evolution scenario (broken line), for the water expulsion scenario (unbroken line) and finally in the case of fissure formation, in which the migration-accessible porosity is 0.12 in case I and 0.012 in case II.</i>	219
<u>Figure 11.5.5-1:</u>	<i>Relative weight of various safety indicators and methods of reasoning.</i>	221
<u>Figure 11.5.5-2:</u>	<i>Activity fluxes to aquifers for vitrified high-level waste (ZAGALC), spent fuel (ZAGALS) and hulls and endpieces (HAGALC2).</i>	222
<u>Figure 11.5.5-3:</u>	<i>Cumulative activity that reaches the aquifer. Radioactive decay in the aquifer is disregarded.</i>	223
<u>Figure 11.5.5-4:</u>	<i>Cumulative quantities of ^{126}Sn released by the different barriers of the disposal system and by its environment for the disposal of 1980 tHM of spent fuel with a burn-up of 55 GWd/tHM.</i>	224
<u>Figure 11.5.5-5:</u>	<i>Cumulative quantities of ^{129}I released by the different barriers of the disposal system and by its environment for the disposal of 1980 tHM of spent fuel with a burn-up of 55 GWd/tHM.</i>	224

Chapter 12

- Figure 12-1:** *The successive phases in the implementation of a disposal system for high-level vitrified waste (ZAGALC) and spent fuel (ZAGALS)..... 225*
- Figure 12-2:** *Schematic representation of changes in retrievability through the different phases of the repository life. 225*

Chapter 13

- Figure 13-1:** *Classification of conditioned radioactive waste in Belgium. While the SAFIR 2 report covers all of the waste in the geological group, it deals more specifically with the long-term management of very high-level vitrified waste and non-reprocessed spent fuel, that is, waste from the Z-classes, these being the most demanding classes in radiological and thermal terms..... 227*
- Figure 13-2:** *Schematic succession (stratigraphy, lithology, and representation for the hydrogeological modelling) of the aquifers and aquitards of the Campine Basin from the Cretaceous to the Quaternary..... 228*
- Figure 13-3** *Resistivity imaging in the Mol-1 borehole and interpretation based on different wireline loggings and observations on site..... 229*
- Figure 13-4:** *Variation in migration parameters for the species HTO and Γ and in hydraulic conductivity over the thickness of the Boom Clay at the site of the Mol-1 borehole. 230*
- Figure 13-5:** *Schematic of the various phases of the programme of deep disposal into the Boom Clay as proposed by ONDRAF/NIRAS (without prejudging the decisions that will be taken on this matter)..... 231*
- Figure 13-6:** *The main phases of the stepwise implementation of a disposal system. 232*
- Figure 13-7:** *Illustration of the long term safety functions and the 'safety reserves' for the different periods of a repository 233*
- Figure 13-8:** *The long-term safety functions of the deep disposal system under study that are considered in the long-term safety assessments for the normal-evolution scenario. 233*
- Figure 13-9:** *The different thicknesses of the Boom Clay layer beneath the Mol-Dessel nuclear zone..... 234*

Posters

<u>Poster 1:</u>	<i>Mol-1. Composite of geophysical measurements. During the final editing of the SAFIR 2 report, the stratigraphy was updated on the basis of a new interpretation and new data. Irregularities in the poster lines are caused by computer file conversions.</i>	<i>235</i>
<u>Poster 2:</u>	<i>Doel 1A / 1B. Composite of geophysical measurements.....</i>	<i>236</i>

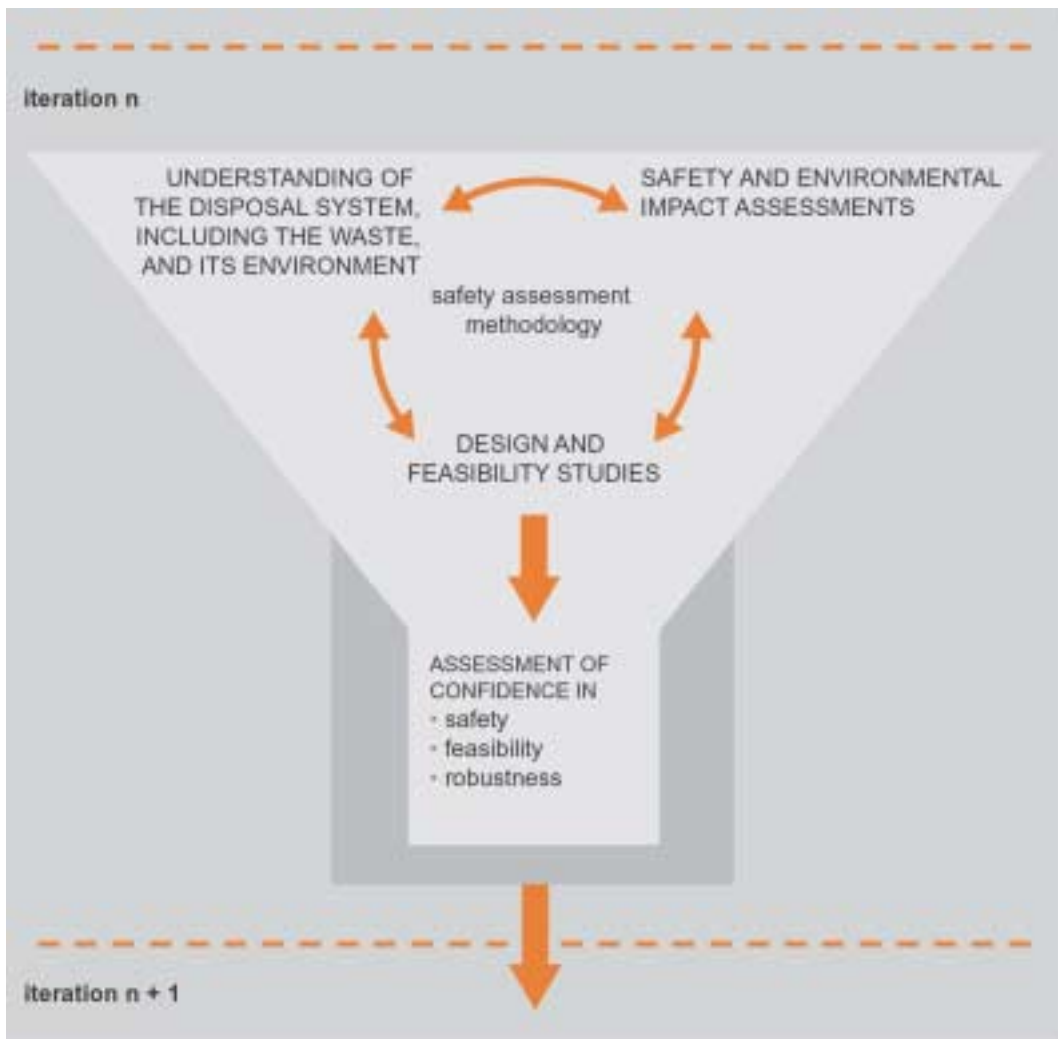


Figure 0-1: *General approach taken by the Belgian methodological research and development programme into deep disposal*

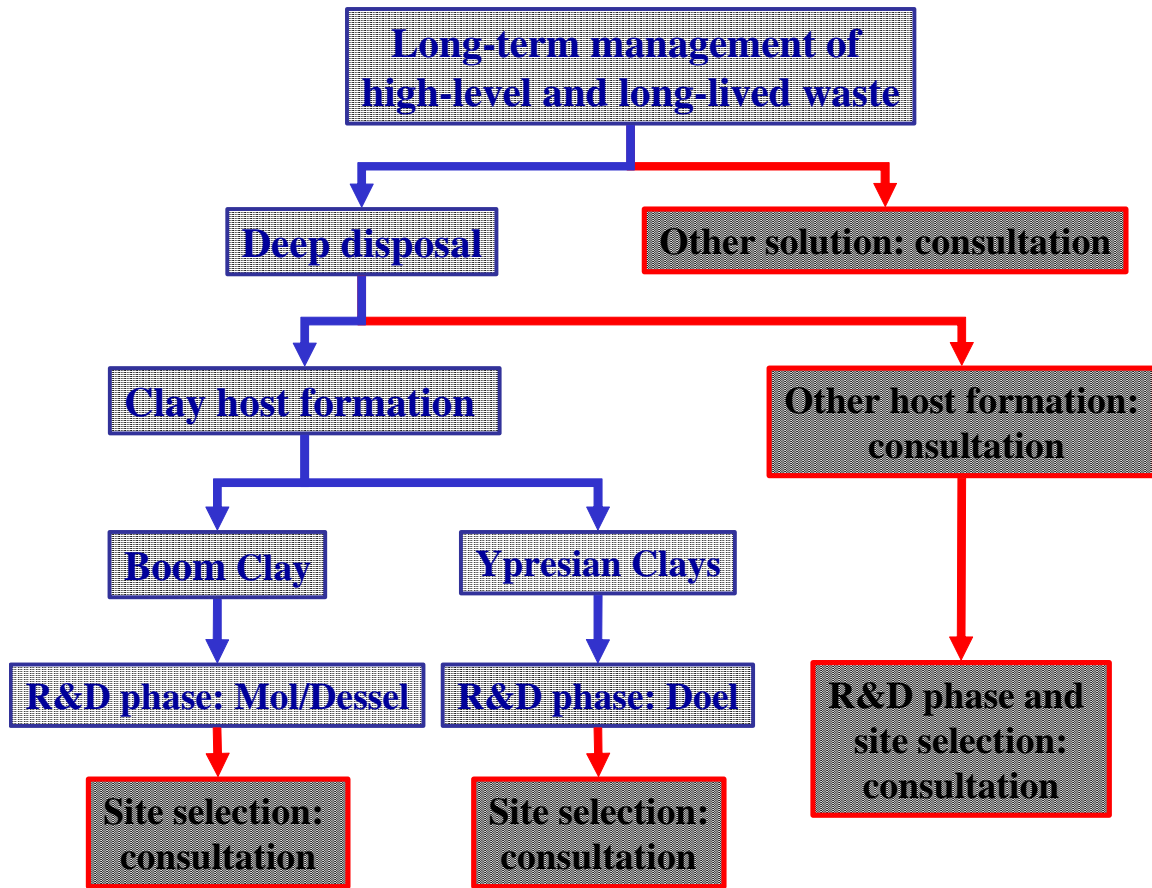


Figure 0-2: *Implicit technical choices made within the methodological R&D programme and within SAFIR 2 (in blue); alternative options are indicated in red.*

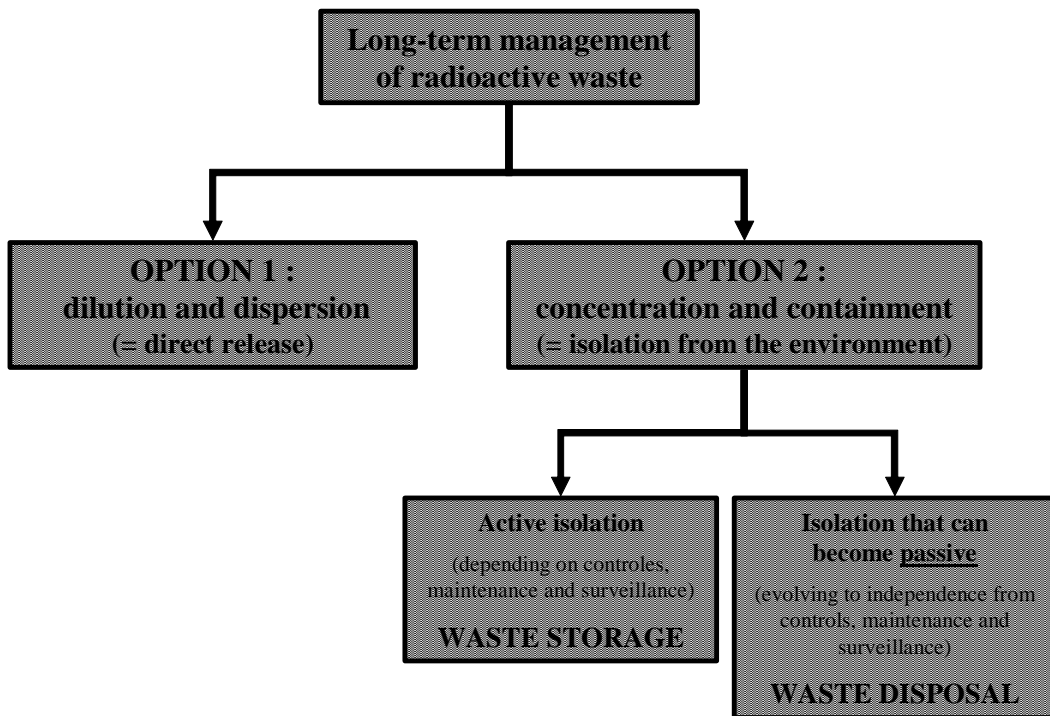


Figure 1-1: Schematic concept of the potential options for the long-term management of radioactive waste

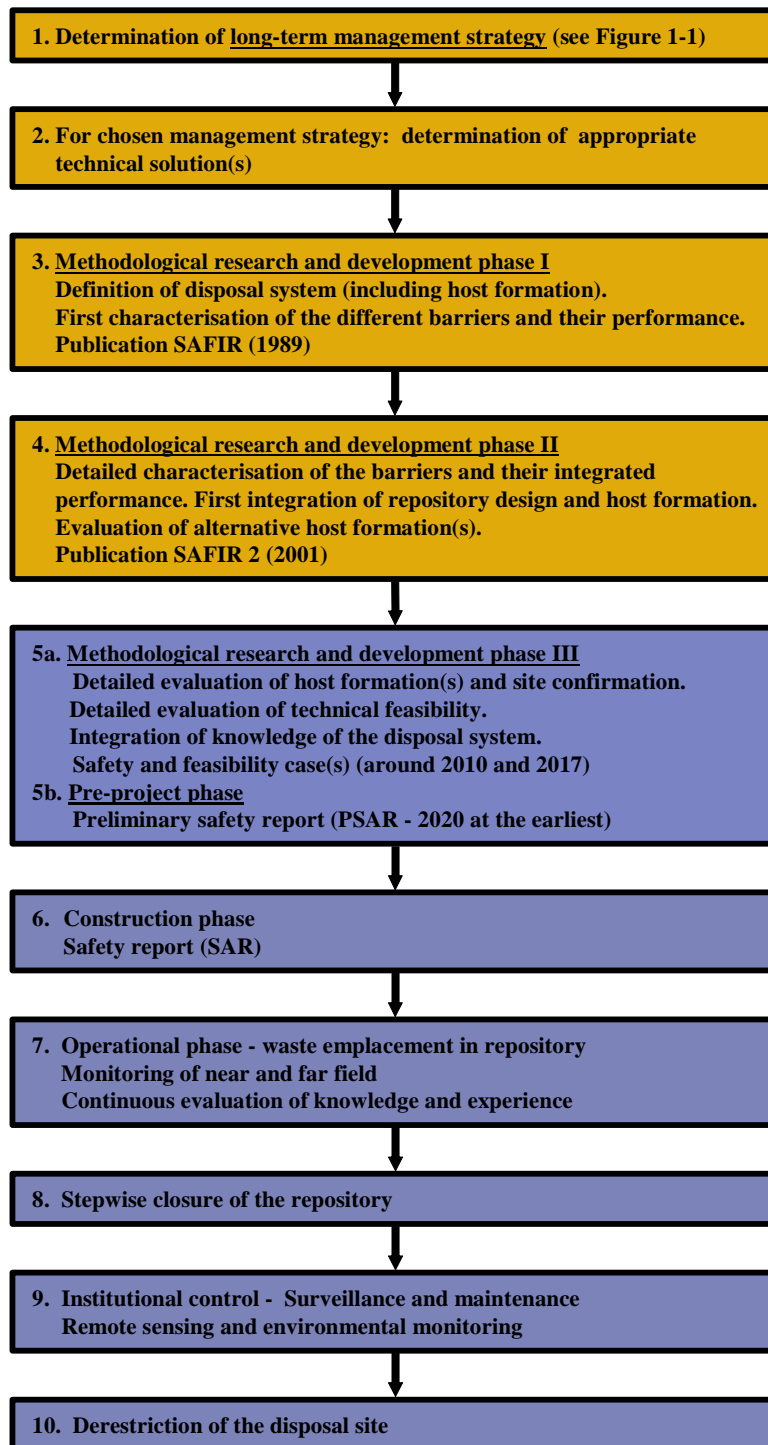


Figure 1-2: *Illustration of the successive phases in the development and implementation of a disposal solution for conditioned high-level and long-lived waste with indicated time scales for a disposal in the Boom Clay Formation.*

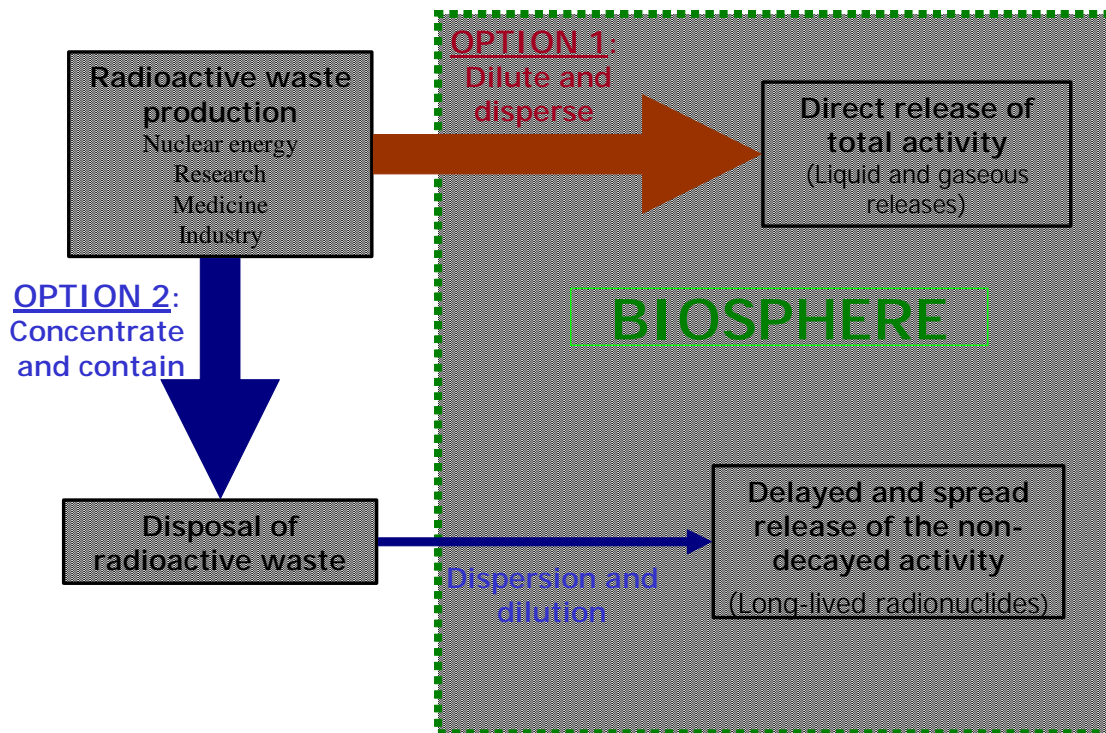


Figure 1-3: Comparison of release to the biosphere resulting from the two management options ‘dilute and disperse’ and ‘concentrate and contain’ (by disposal).

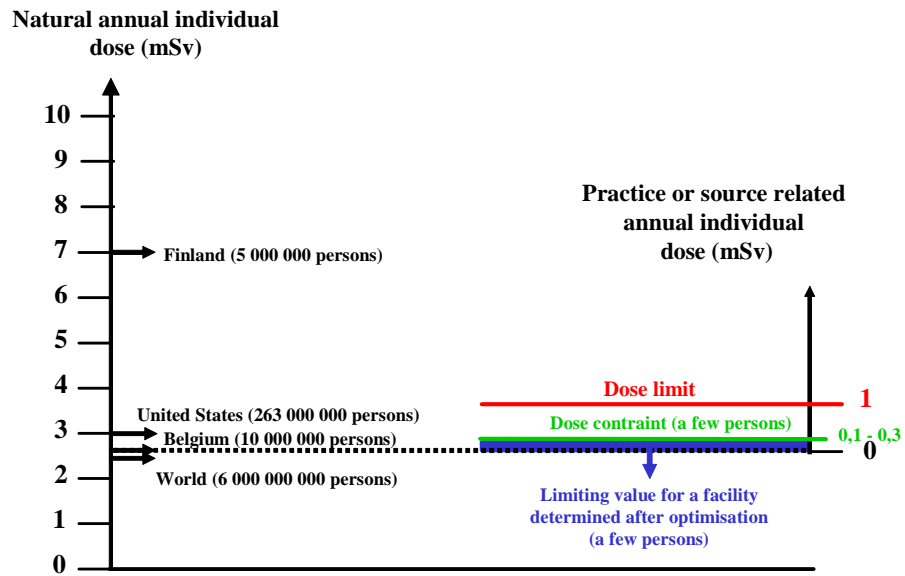


Figure 1-4: Mean annual natural exposure in a number of countries and comparison with the dose limit and dose constraint.

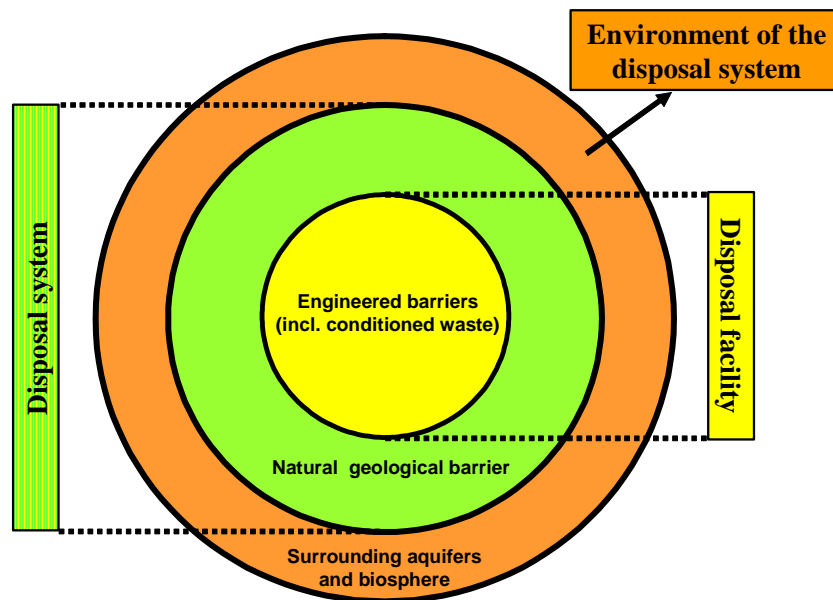


Figure 1-5: The various components and main barriers of the disposal facility and the disposal system.

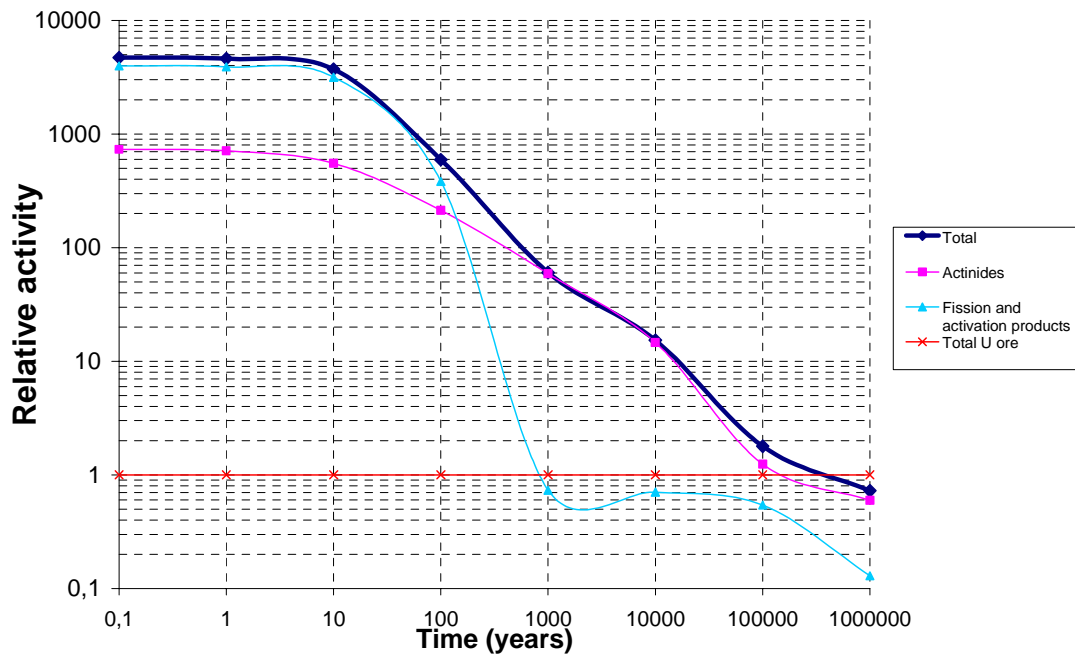


Figure 1-6: *Relative activity of a spent nuclear fuel (burn-up of 45 MWd/kg U) and comparison with the activity of an equivalent amount of uranium ore [25]. The short-lived radionuclides are not considered in this figure.*

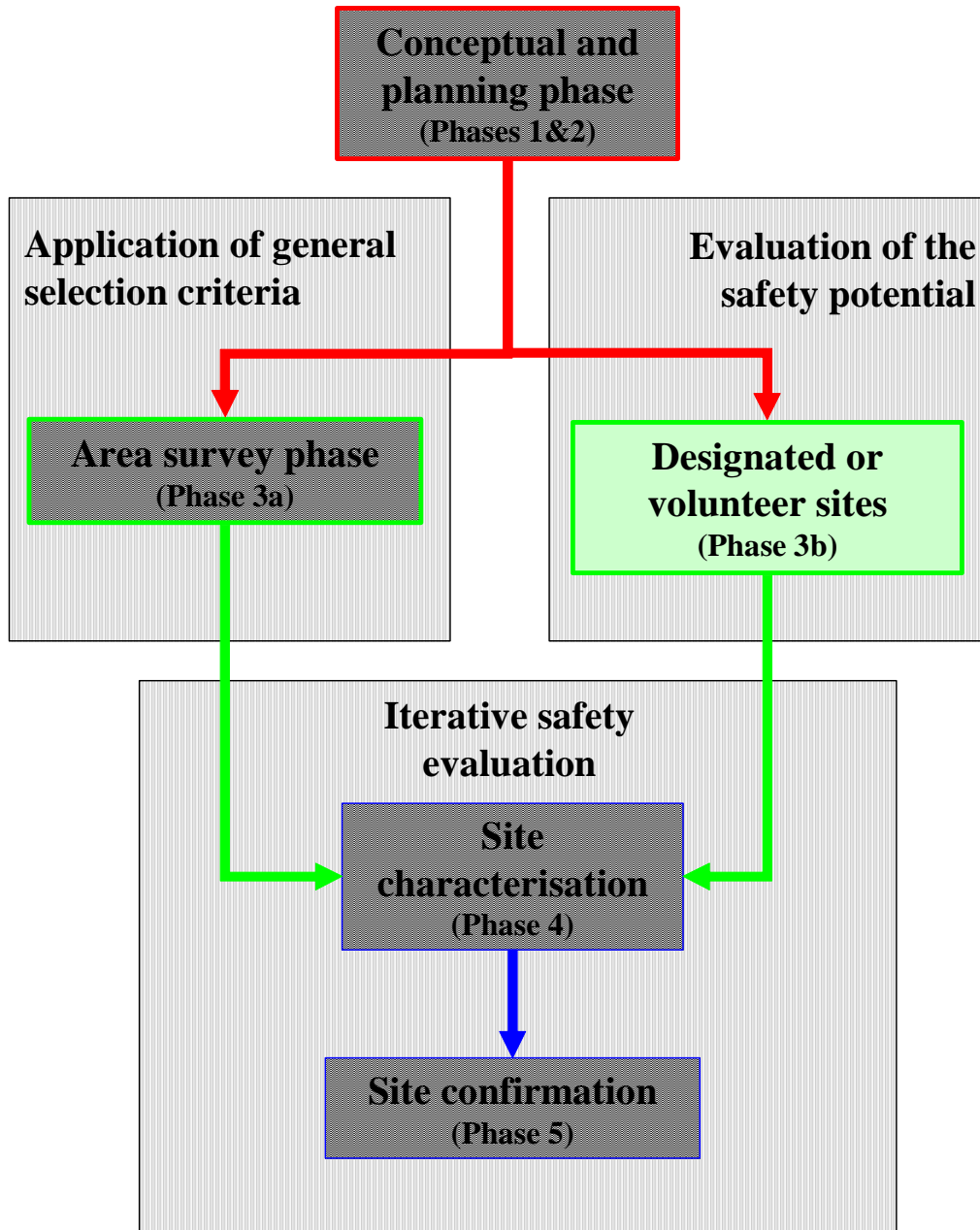


Figure 1-7: Schematic representation of the two approaches to site selection discussed in the text. The phase in Figure 1-2 corresponding to each step in the selection process is also given.